

# High Resolution $\lambda = 2.7$ mm Observations of L1551 IRS5: A Protobinary System?

Leslie W. Looney<sup>1</sup>, Lee G. Mundy<sup>2</sup>

Department of Astronomy, University of Maryland, College Park

and

W. J. Welch<sup>3</sup>

Radio Astronomy Laboratory, University of California, Berkeley

## ABSTRACT

We present sub-arcsecond resolution imaging of the  $\lambda = 2.7$  mm continuum emission from the young, embedded system L1551 IRS5 using the nine-element, high-resolution configuration of the BIMA array. The observed emission arises from two compact sources separated by  $0''.35$ , coinciding with the two sources seen at  $\lambda = 2$  cm and  $\lambda = 1.3$  cm. When the high resolution data is combined with data from two compact configurations, L1551 IRS5 is argued to consist of a protobinary system separated by  $\sim 50$  AU with individual circumstellar disks, a circumbinary structure, and a large-scale envelope. The characteristic masses of the components are:  $0.024 M_{\odot}$  for the northern circumstellar disk,  $0.009 M_{\odot}$  for the southern circumstellar disk,  $0.04 M_{\odot}$  for the circumbinary material, and  $0.28 M_{\odot}$  for the envelope.

*Subject headings:* stars:circumstellar — stars:formation — binaries: close — stars: individual (L1551 IRS5) — Infrared: stars — Radio Continuum: stars

## 1. Introduction

First detected in an infrared survey of the L1551 cloud (Strom, Strom, & Vrba 1976), L1551 IRS5 is a prototypical young stellar system, with a strong bipolar molecular outflow (Snell, Loren, & Plambeck 1980), an optical jet (Mundt & Fried 1983), HH objects (Herbig 1974), and an envelope-disk structure in the surrounding material (Keene & Masson 1990). Located at a distance of 140 pc (Elias 1978) and exhibiting a luminosity of  $\sim 28L_{\odot}$  (Butner *et al.* 1991),

---

<sup>1</sup>Email: lwl@astro.umd.edu

<sup>2</sup>Email: lgm@astro.umd.edu

<sup>3</sup>Email: welch@jack.berkeley.edu

L1551 IRS5 was one of the defining examples for Class I sources in the classification scheme of Adams, Lada, and Shu (1987) and has been used as an archetype in the current paradigm for single-star formation (Shu *et al.* 1993). But is it really a single-star system?

High resolution  $\lambda = 2$  cm continuum observations of L1551 IRS5 show two compact sources with a separation of  $\sim 0''.28$  (Bieging & Cohen 1985; Rodríguez *et al.* 1986) which have been interpreted as either a protobinary system (Bieging & Cohen 1985), or the inner ionized edges of a gas and dust toroid surrounding a single star (Rodríguez *et al.* 1986). The latter is the most widely accepted interpretation, but comparisons with  $\lambda = 2$  cm emission from other young binary systems such as T Tau and Z CMa (Bieging, Cohen, & Schwartz 1984; Schwartz, Simon, & Zuckerman 1983), suggest that the binary interpretation is also viable.

Under the assumption that L1551 IRS5 is a single star system, Keene and Masson (1990) modeled  $\lambda = 2.7$  mm interferometric observations to deduce the presence of a 45 AU radius circumstellar disk within an envelope. This envelope, which extends out  $\sim 1000$  AU from IRS5, contains 0.1 to 1  $M_{\odot}$  of material (Ladd *et al.* 1995; Fuller *et al.* 1995). High resolution JCMT-CSO interferometric observations at  $\lambda = 870 \mu\text{m}$  resolved the compact central emission (Lay *et al.* 1994), and the emission was modeled as arising from an 80 AU radius Gaussian source, inferred to be an accretion disk around the young star.

In this letter, we present sub-arcsecond imaging of the  $\lambda = 2.7$  mm continuum emission from the L1551 IRS5 system. These observations re-open questions about the binarity of the system and the distribution of the surrounding material.

## 2. Observations and Data Reduction

L1551 IRS5 was observed in three array configurations of the 9-element BIMA Array<sup>4</sup> (Welch *et al.* 1996). The longest baselines were 1 km N-S and 900 m E-W, yielding a maximum projected baseline of 480 k $\lambda$  (1.4km); the shortest baselines were limited by the antenna size of 6.1 m, yielding a minimum projected baseline of 2.2 k $\lambda$ . This range in projected baselines provides images with a minimum resolution of  $0''.3$ , fully sampled to sizes as large as  $60''$ .

For the high resolution configuration (March 1, 1996), atmospheric phase fluctuations were tracked by switching the antennas between source, phase calibrator, and a nearby weak quasar on a two minute cycle. The usefulness of this quick switching technique has been demonstrated at the VLA (Holdaway & Owen 1995). The main phase calibrator (0530+135) was used to track rapid atmospheric phase fluctuations. The secondary quasar (0449+113) was used to track slow phase drifts due to the difference in airmass between the primary calibrator and source and, more importantly for this array, phase drifts due to uncertainties in baseline length.

---

<sup>4</sup> The BIMA Array is operated by the Berkeley Illinois Maryland Association under funding from the National Science Foundation.

The digital correlator was configured with two 700 MHz bands centered at 107 GHz and 109 GHz. The flux amplitude calibration assumed a flux of 6.8 Jy for 0530+135, as observed in the following month’s compact array. The coherence of the atmosphere was checked on the quasars; the uncertainty in the amplitude calibration is 20%. Absolute positions in our map have uncertainty due to the uncertainty in the antenna baselines and the statistical uncertainty from the signal-to-noise of the observation. These two factors add in quadrature to give an absolute positional uncertainty of  $0''.14$ . The lower resolution data (acquired on October 3, 1996, February 2, 1997, and March 8, 1997) used 0530+135 to track phase variations and Mars for amplitude calibration.

The L1551 IRS5 data were imaged in four ways which stress structures present on different spatial scales. Figure 1 shows four maps: two with robust weightings of the visibilities (robust = 0.5 yielding a  $3''.25 \times 3''.04$  beam and robust = -0.25 yielding a  $1''.11 \times 0''.84$  beam), one with natural weighting of only the high resolution A array data restored with the fitted “clean” beam ( $0''.73 \times 0''.31$  beam), and one with the A array data restored with a circular  $0''.31$  “clean” beam. The latter technique strongly emphasizes the high resolution information present in the A array  $u,v$  data. With maximum projected baselines ranging from 320 k $\lambda$  to 480 k $\lambda$ , the smallest fringe spacings in our dataset ranges from  $0''.64$  to  $0''.44$ ; hence information down to size scales of  $0''.2$  to  $0''.3$  is present in the  $u,v$  data. High resolution maps of the secondary quasar 0449+113, using the standard technique and using the  $0''.31$  “clean” beam, were consistent with a point source.

### 3. Results

Figure 1a ( $3''$  resolution) has a peak flux of  $122 \pm 3$  mJy beam $^{-1}$ , and the integrated flux in a  $8''$  box centered on the source is  $162 \pm 6$  mJy. A Gaussian fit to the image gives a deconvolved Gaussian source size of  $1''.78 \times 1''.75$  and PA= $68^\circ$ . Figure 1b ( $1''$  resolution) has a peak flux of  $78 \pm 3$  mJy beam $^{-1}$ , and the integrated flux in a  $3''$  box centered on the source is  $143 \pm 10$  mJy. A Gaussian fit to the image gives a deconvolved Gaussian source size of  $0''.92 \times 0''.61$  and PA= $157^\circ$ . Figure 1c shows the map of the A array data alone restored with the Gaussian fitted clean beam. The peak flux in the map is  $45 \pm 5$  mJy beam $^{-1}$ , and the integrated flux in a  $1''.3$  box centered on the source is  $75 \pm 11$  mJy. Although it is not obvious in Figure 1c, over  $\frac{1}{2}$  of the flux present in the lowest resolution map is now gone and the peak flux is roughly  $\frac{1}{3}$  of that in Figure 1a. Despite the elongated “clean” beam, the remaining emission is clearly extended north-south in the CLEANed image; a Gaussian fit to the image gives a deconvolved Gaussian source size of  $0''.53 \times 0''.32$  and PA= $7.2^\circ$ . Figure 1d shows the A array data restored with the circular  $0''.31$  beam. The north-south extension is obvious in this map and there is no hint of east-west extension. The peak flux is  $38$  mJy beam $^{-1}$  corresponding to a brightness temperature of 41 K.

The images in Figure 1a and 1b emphasize the overall emission from the L1551 system. The reconstructions in Figure 1c and Figure 1d highlight the small scale emission which is more compact than expected for the disk size estimates of Keene and Masson (1990) and Lay *et al.*

(1994). The compact emission is consistent with arising from two point sources, as seen at  $\lambda = 2$  cm and  $\lambda = 1.3$  cm (Rodríguez *et al.* 1986; Koerner & Sargent 1997). A two Gaussian fit to the  $\lambda = 2.7$  mm emission in Figure 1d yields the following positions hereafter labeled IRS5 A and IRS5 B: IRS5 A:  $\alpha(\text{J2000}) = 04^{\text{h}}31^{\text{m}}34^{\text{s}}.143$ ,  $\delta(\text{J2000}) = 18^{\circ}08'05''.09$  and IRS5 B:  $\alpha(\text{J2000}) = 04^{\text{h}}31^{\text{m}}34^{\text{s}}.141$ ,  $\delta(\text{J2000}) = 18^{\circ}08'04''.74$ . These positions agree to within  $0''.05$  with the  $\lambda = 1.3$  cm source positions of Koerner and Sargent (1997). The separation of the two sources is  $0''.35$ , corresponding to 49 AU. Both sources have deconvolved sizes of  $\leq 0''.3$ . A two point source fit yields flux densities of  $45 \pm 6$  mJy for IRS5 A and  $23 \pm 6$  mJy for IRS5 B. The total flux density in the compact sources is then  $68 \pm 9$  mJy.

#### 4. Comparisons with Centimeter High Resolution Data

High resolution centimeter wavelength images of L1551 IRS5 show two point-like sources and an extended jet (Bieging & Cohen 1985). The jet is detected only at long centimeter wavelengths; the two point sources dominate the flux at shorter wavelengths. The  $\lambda = 2$  cm flux densities are 1.2 mJy for IRS5 A and 0.93 mJy for IRS5 B (Rodríguez *et al.* 1986). Recent VLA observations also resolved the two sources at  $\lambda = 1.3$  cm (Koerner & Sargent 1997) and yielded flux densities of  $2.0 \pm 0.2$  mJy and  $1.5 \pm 0.2$  mJy, respectively. The spectral indices between  $\lambda = 2.0$  and 1.3 cm are then  $\alpha_A \sim 1.25$  and  $\alpha_B \sim 1.04$ , consistent with  $\alpha \sim 1$  estimated by Bieging and Cohen (1985). Extrapolating to 109 GHz, this emission could contribute as much as  $\sim 14.4$  mJy and  $\sim 7.8$  mJy, respectively, to the observed fluxes. Hence, the  $\lambda = 2.7$  mm flux is dominated by dust emission.

The proposal of Rodríguez *et al.* (1986) that the  $\lambda = 2$  cm emission traces the ionized inner edge of a larger dusty torus is not consistent with the observed compact  $\lambda = 2.7$  mm emission. Since the millimeter emission directly probes the dust, we should easily see the torus in our high resolution maps. If there were a torus, the  $\lambda = 2.7$  mm emission would extend beyond the  $\lambda = 2$  cm sources and, in fact, peak outside of them. The binary interpretation of Bieging & Cohen is consistent with our image if the  $\lambda = 2.7$  mm emission arises from circumstellar disks within the binary system, while the  $\lambda = 2$  cm emission traces ionized gas associated with stellar winds or jets.

#### 5. The Structure of the L1551 IRS5 System

Combining all observations to date, the L1551 IRS5 system consists of three main circumstellar components: a large-scale envelope (Keene and Masson 1990; Ladd *et al.* 1995), a disk or extended structure with a size scale of  $\sim 1''$  (Lay *et al.* 1994; Keene and Masson 1990), and an inner binary system as argued in section 4. How do these components fit together? To answer this question,

we compare our  $u, v$  data binned in annuli with simulated observations of models for the system, binned similarly. In the following subsections we discuss each component and derive characteristic masses.

### 5.1. Binary Circumstellar Disks

Figure 2a compares our  $u, v$  data with the Gaussian model from Lay *et al.* (1994) scaled to match the  $\lambda = 2.7$  mm flux at 50 k $\lambda$ . Above 100 k $\lambda$ , the Gaussian model is resolved out and does not fit the data; below 20 k $\lambda$  the data diverge from the model due to flux from the envelope. Figure 2b shows a two point source model with the separation and amplitudes given in section 3. The two point sources beat together to cause the variations in flux seen past 100k $\lambda$ . The proposed binary disk system is evident only in our data; its separation is too small to be resolved in the data of Lay *et al.* (1994) or Keene and Masson (1990). In fact, due to the small angular size and the embedded nature of the binary system, the properties of the proposed disks are poorly constrained by observations to date. The projected separation and extent of the  $\lambda = 2.7$  mm emission suggests a maximum outer radius of 25 AU for the disks. To estimate the masses of the disks, we assume a standard power-law disk with parameters characteristic of the HL Tau disk,  $T_{disk} = 330(\frac{1AU}{r})^{0.5}$  and  $\Sigma_{disk} \propto r^{-1}$  (Mundy *et al.* 1996; Beckwith & Sargent 1991). For dust properties, we adopt  $\kappa=0.1(\frac{\nu}{1200GHz})$  cm<sup>2</sup> g<sup>-1</sup>, which is consistent with other recent works (e.g. Osterloh and Beckwith 1995; Ohashi *et al.* 1991; Beckwith & Sargent 1991). With these assumptions, the disk masses are  $M_A \sim 0.024 M_{\odot}$  and  $M_B \sim 0.009 M_{\odot}$ .

### 5.2. The Envelope

The excess emission in our robust weighted maps (Figures 1a and 1b) compared to our highest resolution map (Figure 1d) and the rise in flux on baselines shorter than 15 k $\lambda$  (Figure 2), are due primarily to the extended envelope. Our flux densities in the larger beams are consistent with previous measurements at similar resolutions: Keene and Masson (1990) find a peak flux of 130 mJy beam<sup>-1</sup> at  $\lambda = 2.73$  mm in a 2''6 beam and a total flux of 150 mJy; Ohashi *et al.* (1996) measure a total flux of 160 mJy at  $\lambda = 2.73$  mm using a 4''5 beam. Our  $u, v$  data in Figure 2 and Figure 2 of Keene and Masson (1990), show similar fluxes around 10 k $\lambda$ , but our data has 20% to 30% less flux from 40 k $\lambda$  to 70 k $\lambda$ . These differences are within the calibration uncertainties.

The differences in flux densities at different resolutions, or equivalently the drop in flux density with  $u, v$  distance, can be used to estimate the properties of the envelope. Our data are broadly consistent with the envelope parameters determined by Ladd *et al.*(1995) and Fuller *et al.*(1995). Fitting the drop in flux between 2.6 k $\lambda$  and 15 k $\lambda$  with a power-law envelope model ( $\rho(r) \propto r^{-1.5}$  and  $T(r) \propto r^{-0.5}$ ) combined with the two point source model from section 5.1, reasonable results are obtained for an envelope mass of  $\sim 0.44 M_{\odot}$ , an outer radius of  $\sim 1300$  AU, and an inner

envelope radius of 30 AU (Figure 2c). Steeper envelope density laws ( $\rho(r) \propto r^{-2}$ ) also fit the data with a characteristic mass and outer radius of  $0.43 M_{\odot}$  and 1800 AU, respectively.

### 5.3. The Circumbinary Structure

Finally, an intermediate-sized structure, perhaps a circumbinary disk such as seen around GG Tau (Dutrey, Guilloteau, Simon 1994) or a “pseudo-disk” (Galli and Shu 1993), is needed to account for the structure resolved by Lay *et al.* (1994) and the compact structure deduced by Keene and Masson (1990). In our data, this structure is evident as the excess emission between  $30 \text{ k}\lambda$  and  $90 \text{ k}\lambda$  in Figure 2c. As shown in Figure 2d, this excess can be fitted with a Gaussian model consistent with that of Lay *et al.* ( $1''.2 \times 0''.7 \text{ PA} = 160^{\circ}$ ) with a flux of 30 mJy plus an envelope model with a mass of  $0.28 M_{\odot}$  ( $\rho(r) \propto r^{-1.5}$ ) and a radius of 1100 AU. The parameters of the envelope and the circumbinary structure are interdependent and hence only crudely determined. If the circumbinary structure has dust properties similar to the envelope parameters in section 5.2, the circumbinary structure has a rough mass of  $0.04 M_{\odot}$ .

To test the consistency of the above model with the Lay *et al.* (1994) data, we fit two different source structures to their  $\lambda = 870 \mu\text{m}$  data: a single elliptical Gaussian (a single circumstellar disk) and a single elliptical Gaussian with two central point sources (a circumbinary disk with two small circumstellar disks), following the fitting procedure of Lay *et al.* (1994; also see Lay 1994). The model did not include envelope emission since the JCMT-CSO baselines ranged from  $50 \text{ k}\lambda$  to  $200 \text{ k}\lambda$ , where the envelope emission is completely resolved out. The single elliptical Gaussian model fits the  $\lambda = 870 \mu\text{m}$  data very well, with parameters comparable to those found by Lay *et al.* (1994). The addition of two point sources to the single Gaussian model produces as good a fit as the single Gaussian model, but the FWHM of the Gaussian increases slightly. Hence, the data cannot distinguish between the single Gaussian and single Gaussian with point source models. If the circumbinary material is optically thick at  $\lambda = 870 \mu\text{m}$ , the Lay *et al.* data would not even see the embedded circumstellar disks. If the circumbinary material is not optically thick, the Lay *et al.* data place a limit on the flux from the circumstellar disks: at a 95% confidence level the circumstellar disks emit  $\leq 1.3 \text{ Jy}$  at  $\lambda = 870 \mu\text{m}$ .

## 6. Young Binary systems

Our data present the first direct detection of a close, embedded binary system. Proposed wider binary systems have been identified among embedded sources, e.g. IRAS 16293-2422 (Wootten 1989), NGC 1333 IRAS4 (Sandell *et al.* 1991; Lay *et al.* 1995), and L1527 (Fuller, Ladd, & Hodapp 1996), but the number of such systems is actually quite small compared to the number of known embedded sources. Surveys of pre-main sequence (PMS) stars find that binary systems are at least as common among young visible stars as among main-sequence stars (Simon *et al.*

1992; Ghez, Neugebauer & Matthews 1993; Leinert *et al.* 1993; Reipurth & Zinnecker 1993); so binaries should be common among young, deeply embedded systems. That they have not often been seen is probably due to the lack of sub-arcsecond resolution observations which are necessary to resolve close binaries. The separation of the L1551 IRS5 system is near the median separation for main sequence binaries ( $\sim 30$  AU, Duquennoy & Mayor 1991). The low detection rate of wide embedded binaries is in rough agreement with the fraction of main sequence binaries with separations between 300 and several 1000 AU.

L1551 IRS5 also ranks as one of the few close binary systems with significant dust emission associated with both components. Submillimeter wavelength surveys have generally found lesser amounts of dust emission associated with PMS binary systems than with young single stars systems (Simon *et al.* 1992, 1995). In a statistical comparison of binaries and single stars, Jensen, Mathieu & Fuller (1996) found that binaries with separations  $\leq 50$ -100 AU statistically have lower submillimeter fluxes than wider binaries, but wide binaries are indistinguishable from single stars; hence, the L1551 IRS5 system may be unusual. However, these studies concentrate on T Tauri stars and exclude the youngest sources, Class I or younger. It is possible that embedded close binaries, which are still accreting mass, have substantial circumstellar or circumbinary disks which disappear later when the envelope is no longer feeding-in material.

## 7. Conclusions

Sub-arcsecond  $\lambda = 2.7$  mm observations of L1551 IRS5 have resolved a compact central structure, which is most plausibly interpreted as a young binary system. The  $\lambda = 2.7$  mm continuum emission shows two peaks which are similar, in absolute position and separation, to the free-free emission observed at centimeter wavelengths. Our interpretation is that we are detecting thermal dust emission from small disks around the individual stars in a binary system and that the centimeter emission arises in the associated stellar winds. We propose that the L1551 IRS5 system is composed of two circumstellar disks, located inside a circumbinary structure, embedded in a large-scale envelope. Simple modeling yields masses for these components: circumstellar disk masses of  $0.024 M_{\odot}$  and  $0.009 M_{\odot}$  for the northern and southern sources respectively, a circumbinary structure mass of  $0.04 M_{\odot}$ , and an envelope mass of  $0.28 M_{\odot}$ . The binary separation for L1551 IRS5 is about 50 AU, close to the median separation for main sequence binaries. The small number of young embedded binaries detected to date, probably reflects the inadequate angular resolution available in the earlier studies, rather than an intrinsic sparsity of binaries.

We thank the Hat Creek staff for their efforts in the construction and operation of the long baselines array. We also thank the referee, Jocelyn Keene, and Oliver Lay for their comments. This work was supported by NSF Grants NSF-FD93-20238 and AST-9314847. LGM acknowledges support from NASA grant NAGW-3066.

## REFERENCES

- Adams, F.C., Lada, C.J., & Shu, F.H. 1987, *ApJ*, 312, 788
- Beckwith, S.V.W., & Sargent, A.I. 1991, *ApJ*, 381, 250
- Biegging, J., Cohen, M., & Schwartz, P.R. 1984, *ApJ*, 282, 699
- Biegging, J., & Cohen, M. 1985, *ApJ*, 289, L5
- Butner, H.M. *et al.* 1991, *ApJ*, 376, 636
- Dutrey, A., Guilloteau, S., & Simon, M. 1994, *A&A*, 286, 149
- Duquennoy, A., & Mayor, M. 1991, *A&A*, 248, 485
- Elias, J. 1978, *ApJ*, 224, 857
- Fuller, G.A., Ladd, E.F., & Hodapp, K.W. 1996, *ApJ*463, L97
- Fuller, G.A., Ladd, E.F., Padman, R., Myers, P.C., & Adams, F.C. 1995, *ApJ*, 454, 862
- Galli, D., & Shu, F. 1993, *AJ*417, 243
- Ghez, A.M., Neugebauer, G., Matthews, K. 1993, *AJ*, 106, 2005
- Herbig, G. H. 1974, *Lick Observatory Bulletin No.* 658
- Holdaway, M.A., & Owens, F.N. 1995, *NRAO. Millimeter Array Memo* 126.
- Jensen, E.L.N., Mathieu, R.D., & Fuller, G.A. 1996, *ApJ*, 458, 312
- Keene, J., & Masson, C.R. 1990, *ApJ*, 355, 635
- Koerner, D., & Sargent, A.I. 1997, *in preparation*
- Lay, O.P., Carlstrom, J.E., & Hills, R.E. 1995, *ApJ*, 452, 73L
- Lay, O.P., Carlstrom, J.E., Hills, R.E., & Philips, T.G. 1994, *ApJ*, 434, L75
- Lay, O.P. 1994, *Ph.D. Thesis, Cambridge Univ.*
- Ladd, E.F., Fuller, G.A., Padman, R., Myers, P.C., & Adams, F.C. 1995, *ApJ*, 439, 771
- Leinert, C. *et al.* 1993, *A&A*, 278, 129
- Mundt, R., & Fried, J.W. 1983, *ApJ*, 274, L83
- Mundy, L.G. *et al.* 1996, *ApJ*, 464, L169
- Ohashi, N., Hayahi, M., Ho, P.T., Momose, M., & Hirano, N. 1996, *AJ*, 466, 957
- Osterloh, M., & Beckwith, S.V.W. 1995, *ApJ*, 439, 288
- Reipurth, B., & Zinnecker, H. 1993, *A&A*, 278, 81
- Rodríguez, L.F., Cantó, J., Torrelles, J.M., & Ho, P.T.P. 1986, *ApJ*, 301, L25
- Sandell, G., Aspin, C., Duncan, W.D., Russell, A.P.G., & Robson, E.I. 1991, *ApJ*, 376, L17
- Schwartz, P.R., Simon, T., & Zuckerman, B. 1983, *Rev. Mex. Astr. Ap.*, 7, 191

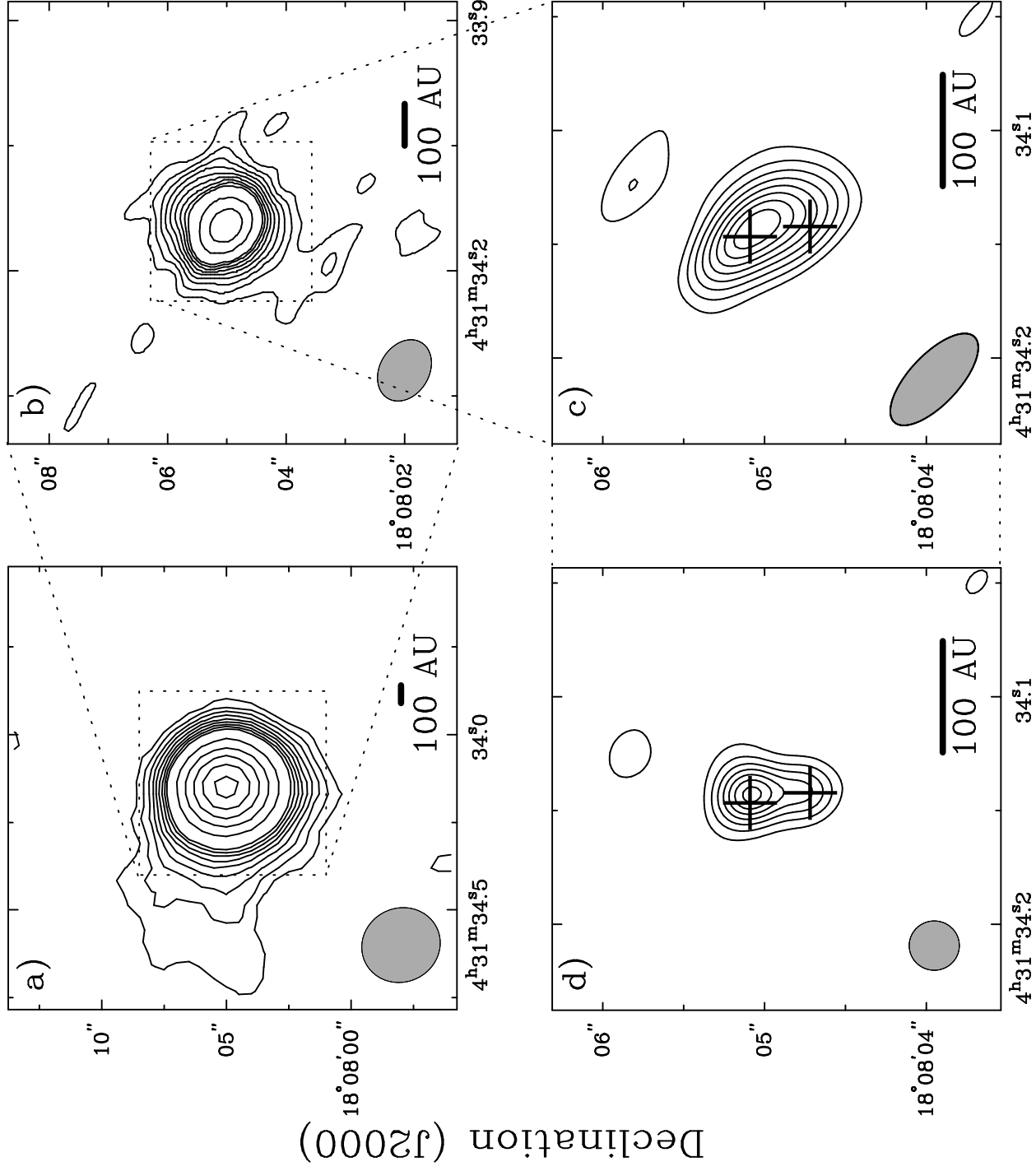


- Shu, F., Najita, J., Galli, D., Ostriker, E., & Lizano, S. 1993, *Protostars and Planets III*, ed. E.H. Levy and J.I. Lunine, Tucson, Univ. of Arizona Press, 3
- Simon, M. *et al.* 1995, ApJ, 443, 625
- Simon, M., Chen, W.P., Howell, R.R., Benson, J.A., & Slowik, D. 1992, ApJ, 384, 212
- Snell, R.L., Loren, R.B., & Plambeck, R.L. 1980, ApJ, 239, L17
- Strom, K.M., Strom, S.E., & Vrba, F.J. 1976, AJ, 81, 320
- Welch *et al.* 1996, PASP, 108, 93
- Wootten, A. 1989, ApJ, 337, 858

Fig. 1.—  $\lambda = 2.7$  mm maps of the continuum emission from L1551 IRS5. a) Robust weighting of 0.5 map made with data from three arrays. The beam is  $3''.25 \times 3''.04$  PA =  $29^\circ$ , and the RMS noise is  $2.5 \text{ mJy beam}^{-1}$ . The contours are -3,-2,2,3,4,5,6,7,8,9,10,15,20,25,30,35 times  $3.3 \text{ mJy beam}^{-1}$  (the RMS from Panel b). b) Robust weighting of -0.25 map made with data from three arrays. The beam is  $1''.11 \times 0''.84$  PA =  $60^\circ$ , and the RMS noise is  $3.3 \text{ mJy beam}^{-1}$ . The contours are the same as in Panel a. c) Naturally weighted map made from only the A array data. The beam is  $0''.73 \times 0''.31$  PA= $47^\circ$  and the RMS is  $4.5 \text{ mJy beam}^{-1}$ . The contours are in steps of  $1 \sigma$  starting at  $\pm 2 \sigma$ . d) A array naturally weighted data, restored with a circular  $0''.31$  beam. The contours and RMS are the same as in Panel c. The two crosses in Panels c and d mark the  $\lambda = 1.3$  cm source positions from Koerner & Sargent 1997. The restoring beam in each panel is shown in the lower left-hand corner.

Fig. 2.— The measured  $\lambda = 2.7$  mm visibilities binned in annuli (open squares) compared with different model visibilities (gray, closed squares). a) The Lay *et al.* (1994) model Gaussian scaled to match the  $\lambda = 2.7$  mm fluxes around  $50 \text{ k}\lambda$ . b) Two point source model constrained by fitting Figure 1d. c) Characteristic model fit with an envelope ( $0.44 M_{\odot}$ ,  $\rho(r) \propto r^{-1.5}$ ,  $T(r) \propto r^{-0.5}$ , and 1300 AU radius) and the two point sources from Panel b. d) Characteristic fit for a model with an envelope ( $0.28 M_{\odot}$ ,  $\rho(r) \propto r^{-1.5}$ ,  $T(r) \propto r^{-0.5}$ , and 1100 AU radius), a Gaussian ( $30 \text{ mJy}$ ,  $1''.2 \times 0''.7$  PA =  $160^{\circ}$ ), and the two point sources from Panel b.

# L1551 IRS5 $\lambda = 2.7$ mm Emission



Right Ascension (J2000)

# L15551 IRS5 $\lambda = 2.7$ mm Visibilities

